Coupling effects between pantograph of high-speed train and tunnel

Zhanling Ji, Yi Guo, Dilong Guo, Guowei Yang & Lingfang Zhang

Published online: 30 May 2022.

Submit your article to this journal ⬈

View related articles ⬈

View Crossmark data ⬈

IA**VSD**

Taylor & Francis
Taylor & Francis Group

Check for updates

Coupling effects between pantograph of high-speed train and tunnel

Zhanling Ji, Yi Guo, Dilong Guo, Guowei Yang and Lingfang Zhang

Institute of Mechanics, Chinese Academy of Sciences, Beijing, People's Republic of China

ABSTRACT

Compression and expansion waves are generated as a train enters a tunnel at high speed. The waves ceaselessly pass through a pantograph as they propagate back and forth in the tunnel; air flow sharply jumps at the exit of the tunnel. The interaction between the pantograph and its surrounding air is significant. In this study, a precise and highly efficient coupling method between aerodynamics and multibody dynamics was developed. The proposed method was verified using line test data. Comparative analyses were conducted between open-air coupling and tunnel coupling, with coupled or non-coupled aerodynamics and multi-body dynamics passing through a tunnel. Some coupling characteristics in time and frequency domains, such as the aerodynamic lift of the panhead, the contact force between pantograph and catenary, and the vertical displacement and acceleration of contact strip, were investigated to clarify the dynamic coupling behaviours and characteristic evolution laws of the pantograph, as well as the coupling effect between the pantograph and tunnel. The results of this work may provide a sound theoretical basis for further improving the current collection quality from the source.

1. Introduction

Railways are crucial national infrastructures and popular means of transportation for many individuals. A nation's railway is the backbone of its transportation system. Development across global economies and industries has driven advancements in railway transportation such as high speed, heavy load, and comfort. These advancements have created stricter requirements for pantograph-catenary current collection quality.

The pantograph, as an articulated mechanical component, relies on its own structure to maintain contact with the contact wire and is susceptible to dynamic forces. The relatively large tunnel-to-line ratio in China creates issues with pantographs passing through tunnels. When the head car and tail car of a train move into the tunnel at high speed, compression and expansion waves are generated, respectively. They are reflected in opposite forms at the entrance and exit of the tunnel. A very complex wave system in the tunnel forms, which ceaselessly passes through the pantograph. This phenomenon is particularly

---

CONTACT Yi Guo ✉ guoyi0536@163.com

intense at the tunnel exit due to the significant differences between the interior and exterior of the tunnel, and is accompanied by a micro pressure wave; the pantograph is thus subjected to violently alternating aerodynamic loads. The dynamic action of the air around the pantograph becomes increasingly significant as train speed increases, so the vibration behaviours of the pantograph become more complicated. The violent vibration of the pantograph also alters its surrounding flow field. As a result, the dynamic service performance of the pantograph sharply drops and the quality of the current collection degrades. In severe cases, the pantograph and the catenary separate and form an electric arc. A massive quantity of heat energy is released instantaneously and the contact strip is ablated, which affects the traction power supply performance of the train. At this point, the train cannot collect current normally.

Many previous researchers have explored pantograph behaviours based on aerodynamics or structural dynamics. Li et al. [1–3], for example, studied the effect of strip spacing on the aerodynamic or aerodynamic noise characteristics of high-speed train pantographs. He et al. [4] simulated the dynamic behaviours of a pantograph-catenary system based on the parametric variational principle and the time-domain integration method. Song [5] studied the influence of the contact surface on the dynamic performance of a pantograph-catenary system. Van et al. [6] discussed the effects of wave expansion and catenary mode on the dynamic behaviours of a pantograph-catenary system. Gregori et al. [7] established coupling equations for the pantograph-catenary system, and proposed a two-stage offline and online method for operating them which shows low calculation cost without loss of precision. Lee et al. [8] introduced effective contact elements and interaction models into pantograph-catenary coupling. Navik et al. [9] predicted the contact force of a pantograph-catenary system via mathematical model. Wang et al. [10] explored pantograph-catenary coupling considering the wear irregularity of the contact wire. Most previous studies have adopted the three-mass model for the pantograph and considered relatively few factors regarding the dynamic performances of the pantograph-catenary system.

Ambient wind and the strong airflow acting on the pantograph are often considered the external loads varying with time. The influence of structural displacement of the pantograph on surrounding air is generally ignored. For example, Carnevale [11] first calculated aerodynamic lift, then estimated the influence of the lift on the contact force between a pantograph and catenary. Considering track excitation, Pombo et al. [12] established a coupling model of the multi-rigid-body pantograph and flexible catenary in interactive mode. However, aerodynamic loads were applied to the rods of the pantograph and the finite element grids of the catenary as external loads. Kulkarni et al. [13] studied the differences in contact force between a pantograph and catenary with versus without the consideration of cross wind, where cross wind was taken as a known load. By using aerodynamic loads as known loads, Song et al. [14] studied the wind-induced vibration response of the catenary at different wind speeds and angles, and the contact force between the pantograph and catenary is affected by random wind. Li [15] applied aerodynamic loads to calculate a pantograph, then studied the coupling characteristics between the pantograph and catenary with or without tunnel effects. Shi et al. [16] investigated the effect of parameters on three-dimensional (3D) pantograph-catenary dynamics under cross wind, which was taken as a known load. When the train exits the tunnel at high speed, the coupling effect between the pantograph and its surrounding air is enhanced, and unidirectional coupling between aerodynamics and dynamics no longer reflects the interaction between them.

Nakade [17] studied the lateral vibration of a high-speed train passing through a tunnel by loose, bidirectional coupling between aerodynamics and structural dynamics. Li et al. [18] adopted an improved algorithm in MATLAB/Simulink under cross wind of open air, where the multi-body dynamic calculation was not carried out until the aerodynamic calculation converged. The dynamic solution programme was embedded into the fluid calculation to avoid to transmit information and wait. The spring approximation method and grid remeshing were adopted to update the grid alongside mesh reconstruction, which may reduce grid quality and computational efficiency, and the train was considered to be stationary. Therefore, this model is not suitable for unsteady flow cases with moving boundaries or two vehicles passing each other.

There have been few previous studies on the coupling between aerodynamics and multi-body dynamics for pantographs. The interaction between the articulated pantograph and its surrounding air cannot be ignored when the train passes through the tunnel at high speed. Therefore, for a 3D pantograph, it is necessary to develop a high-efficiency and high-precision coupling method between aerodynamics and multi-body dynamics.

2. Mathematical modelling

The pantograph consists of two contact strips, two supports of contact strip, a bracket, an upper arm, a lower arm, an upper pull rod, a lower pull rod, and a base frame, which are all regarded as rigid bodies (Figure 1). The contact strips and their supports are fixed together. The contact strip supports are connected to the bracket by two springs. The base frame is fixed to the ground. A spring lifting the pantograph is fixed on the base frame, which connects the base frame and the lower arm. The other connections are hinged joints.

2.1. Multi-body dynamics equation

The multi-body dynamics model of the pantograph is shown in Figure 1. The vertical dynamics equation for each rod of the pantograph is

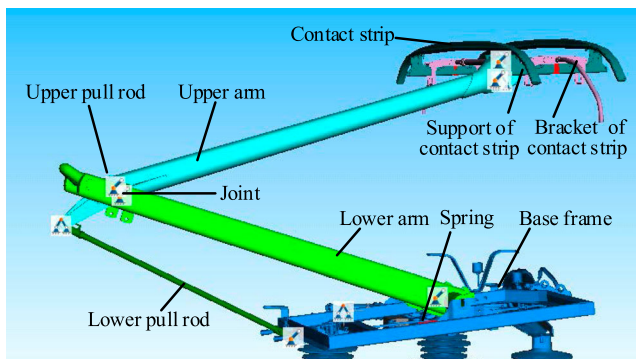$$m\ddot{u} + c\dot{u} + ku = F_n + F_A + F_{link} \qquad (1)$$

Figure 1. Structural components of the pantograph.

where m is the rod mass, c is the rod damper, k is the rod stiffness, u is the vertical displacement of the rod, F_n is the contact force between pantograph and catenary for the contact strip, F_n is 0 for other rods, F_A is the aerodynamic force, and F_{link} is the action force from the connecting rods.

The contact force between the pantograph and catenary is

$$F_n = \begin{cases} k(x)r^{n(x)} + c(x)\dot{r}step(r - d) & r > 0 \\ 0 & r \leq 0 \end{cases} \tag{2}$$

where x is the longitudinal displacement of the contact strip, $x = vt$, v is the running speed of the train, t is running time; the distance between contact strip and catenary $r = u_s - w_0$, u_s is the vertical relative displacement between contact strip and contact wire, w_0 is the unsmoothness of the catenary, $w_0(t) = 0.0055|\sin(2\pi vt/9.5)|$, $d = 0.0005\text{m}$, $n(x) = 1$, and stiffness $k(x) = 7000 - (7000 - 5200)|\sin(\pi vt/9.5)|\text{N/m}$; damper $c(x) = k(x)/100$.

2.2. Governing equation for fluid

The Navier-Stokes equation can be used to describe the flow field relevant to the aerodynamics of high-speed trains. In a Cartesian coordinate system, if the mass force is neglected, the conservative Navier-Stokes equation can be written in the following vector form

$$\frac{\partial \mathbf{U}}{\partial t} + \frac{\partial (\mathbf{E} - \mathbf{E}_v)}{\partial x} + \frac{\partial (\mathbf{F} - \mathbf{F}_v)}{\partial y} + \frac{\partial (\mathbf{G} - \mathbf{G}_v)}{\partial z} = 0 \tag{3}$$

where $\mathbf{U}$, $\mathbf{E}$, $\mathbf{F}$, and $\mathbf{G}$ are the conserved variables and convective fluxes in x, y, and z directions, respectively, which are expressed as follows

$$\mathbf{U} = \begin{pmatrix} \rho \\ \rho u \\ \rho v \\ \rho w \\ \rho e \end{pmatrix}, \quad \mathbf{E} = \begin{pmatrix} \rho u \\ \rho u^2 + p \\ \rho uv \\ \rho uw \\ (\rho e + p)u \end{pmatrix}, \quad \mathbf{F} = \begin{pmatrix} \rho v \\ \rho vu \\ \rho v^2 + p \\ \rho vw \\ (\rho e + p)v \end{pmatrix}, \quad \mathbf{G} = \begin{pmatrix} \rho w \\ \rho uw \\ \rho vw \\ \rho w^2 + p \\ (\rho e + p)w \end{pmatrix} \tag{4}$$

$\mathbf{E}_v$, $\mathbf{F}_v$, and $\mathbf{G}_v$ are the viscous fluxes in x, y, and z directions, respectively, which are expressed as follows

$$\mathbf{E}_v = \begin{pmatrix} 0 \\ \tau_{xx} \\ \tau_{xy} \\ \tau_{xz} \\ u\tau_{xx} + v\tau_{xy} + w\tau_{xz} - q_x \end{pmatrix}, \quad \mathbf{F}_v = \begin{pmatrix} 0 \\ \tau_{xy} \\ \tau_{yy} \\ \tau_{yz} \\ u\tau_{yz} + v\tau_{yy} + w\tau_{yz} - q_y \end{pmatrix},$$

$$\mathbf{G}_v = \begin{pmatrix} 0 \\ \tau_{xz} \\ \tau_{zy} \\ \tau_{zz} \\ u\tau_{zx} + v\tau_{zy} + w\tau_{zz} - q_z \end{pmatrix} \tag{5}$$

The stress terms are expressed as follows:

$$\tau_{xx} = 2\mu u_x - \frac{2}{3}\mu(u_x + v_y + w_z); \tau_{xy} = \tau_{yx} = \mu(u_y + v_x);$$

$$\tau_{yy} = 2\mu v_y - \frac{2}{3}\mu(u_x + v_y + w_z); \tau_{zz} = 2\mu w_z - \frac{2}{3}\mu(u_x + v_y + w_z);$$

$$\tau_{yz} = \tau_{zy} = \mu(v_z + w_y); \tau_{xz} = \tau_{zx} = \mu(u_z + w_x) \tag{6}$$

and the heat conduction items are expressed as follows

$$q_x = -k\frac{\partial T}{\partial x}; q_y = -k\frac{\partial T}{\partial y}; q_z = -k\frac{\partial T}{\partial z} \tag{7}$$

In Equations (3)–(7), u, v, and w are the directional components of air velocity; p, T, k, and e are the pressure, temperature, heat conduction coefficient, and internal energy of air, respectively; μ is a viscosity coefficient.

The total energy e per unit mass of air is

$$e = \frac{p}{(\gamma - 1)\rho} + \frac{u^2 + v^2 + w^2}{2} \tag{8}$$

where γ is the specific heat ratio.

In order to close the Navier-Stokes equation, it is also necessary to supplement the complete gas state equation:

$$p = \rho RT \tag{9}$$

3. Coupling between aerodynamics and multi-body dynamics

3.1. Coupling method

A flow chart of the coupling method between aerodynamics and multi-body dynamics for high-speed pantographs is shown in Figure 2. An aerodynamics calculation model is first established for the pantograph (including three cars). To simulate the train moving to the ground, the flow field is divided into an inner field and outer field. Data are exchanged by defining interfaces between them. The moving parts are defined by self-defining grid motion. A multi-body dynamics model of the pantograph is then established, wherein different disturbances can be considered. The calculated results of the two subjects are exchanged. The dual-time step is used and results are exchanged multiple times in one physical time step. The data exchanged at a given time point can be approximately considered as the data of the current time step, which minimises any temporal error using the results of the previous time step in the current time step. The next time step is not calculated until the predetermined accuracy or predetermined times is reached.

Compared with the direct coupling method [19], the proposed method more easily converges to satisfy engineering requirements when there is a strong interaction between aerodynamics and structural dynamics. Compared with the unidirectional coupling method [11–16] or loose coupling method [17,20], it also has better calculation time precision. In a previous study conducted in our laboratory [21], we used formula derivation to compare the calculation precision between loose coupling and tight coupling. When loose coupling
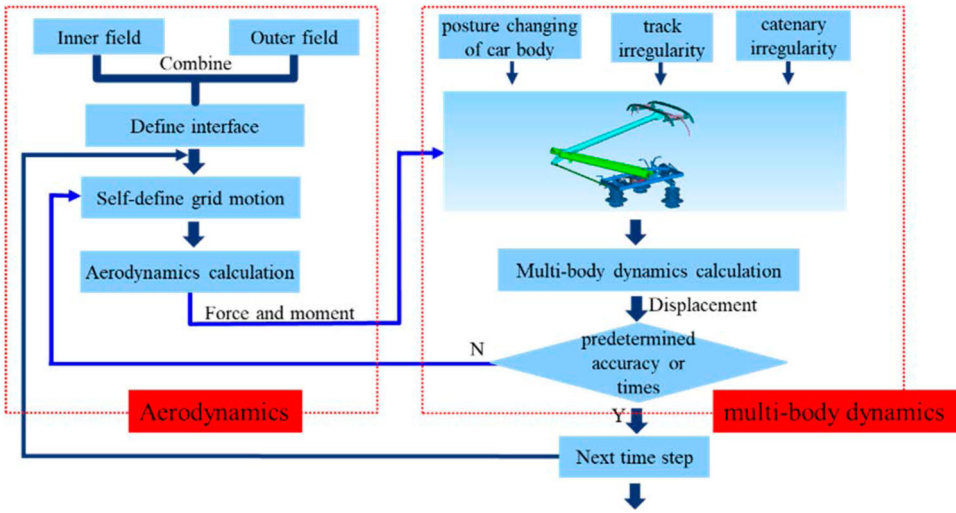
Figure 2. Flow chart of the coupling between aerodynamics and multi-body dynamics adapting to high-speed pantographs.
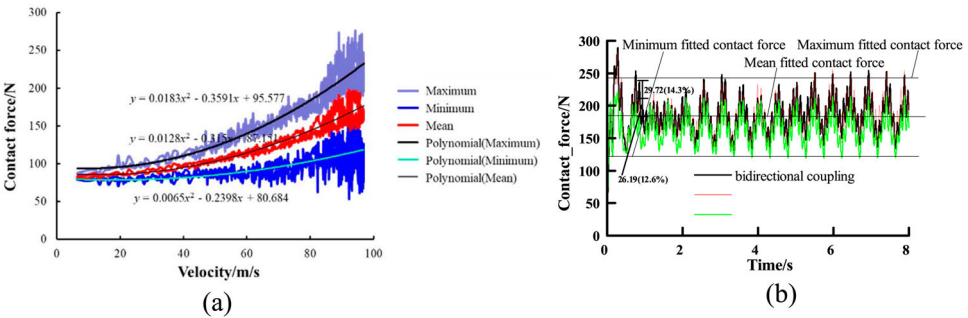

Figure 3. Contact force between pantograph and catenary simulated, tested and fitted under the case of open air (a) Contact force tested and fitted at different speeds; (b) Contact force simulated at 360 km/h.

is used, the overall time accuracy is only first-order. When tight coupling is used, the overall time accuracy is second-order if both structure and fluid have second-order accuracy. Unlike the overlapping grid motion method [22–24], there is no need to reserve gaps or add collar meshes among the rods as they rotate (i.e. cross wall boundaries) and there is no isolated element problem.

3.2. Verification of proposed coupling method

At different train speeds under open air, the maximum, minimum, and mean values of contact force between pantograph and catenary were tested on the actual line. The fluctuation range of contact force increases as speed increases. In order to properly utilise the measurements, they were fitted by the polynomials as shown in Figure 3(a). At 100 m/s, the maximum, minimum and mean values of contact force were calculated by the polynomials to obtain the 'fitted results', which are listed in Table 1.

Table 1. Statistical results of the contact force between pantograph and catenary simulated and fitted under open air at 360 km/h.

	Maximum	Minimum	Mean	Standard deviation	Mean error	Minimum error
Bidirectional coupling	254.264	126.475	183.55598	25.55415	−0.05%	3.92%
Aerodynamics loads as known loads	255.9772	129.57878	182.58699	25.02823	−0.58%	6.47%
No aerodynamics loads	216.15146	119.43517	162.41813	21.661	11.56%	−11.56%
Fitted results	242.667	121.704	183.65	–	–	–

A simulation analysis of the pantograph was conducted in order to verify the proposed coupling method based on test results. Speed was set to 360 km/h, conditions were open air, and the influence of the car body on the flow field was considered. The contact forces between pantograph and catenary are shown in Figure 3(b) when aerodynamics and multi-body dynamics are coupled (i.e. 'bidirectional coupling'), aerodynamics loads are taken as known loads and aerodynamics loads are not considered. The initial stage was removed when the statistical results of the contact force were calculated for a strict comparison against the test results. The stable-state statistics are given in Table 1, where all the proportions listed are based on the fitted results.

As shown in Figure 3 and Table 1, under the three cases investigated here, the change laws of contact force between the pantograph and catenary are basically the same; aerodynamics loads only change the values. Compared with the other two cases, when the aerodynamic loads are not considered, the values and the fluctuation ranges of contact force are much smaller. To this effect, the aerodynamics loads significantly impact the pantograph current collection when the train runs at high speed. Unlike when aerodynamic loads are considered known loads, under the coupling between aerodynamics and multi-body dynamics, the standard deviation of contact force is slightly larger; contact force fluctuates a little greatly and the current collection quality is relatively poor. Regardless of the maximum, the minimum, or the mean, the results calculated by the coupling method are closer to the test results than under other cases.

3.3. Verification of grid independence

In order to verify the grid independence for aerodynamics calculation, the pantograph was divided into three sets of grids with a high-speed train passing through a tunnel. The total cells are 24 million, 14 million, and 10 million, respectively. At the stable stage of open air, the calculation results for drag coefficient, lateral force coefficient, and lift coefficient from the pantograph are shown in Table 2. The results of the medium grid are closer to that of the fine grid than the coarse grid. Therefore, to ensure computational accuracy and improve calculation efficiency, a medium grid was utilised for all subsequent analyses.

Table 2. Aerodynamic coefficient of the pantograph with different grid numbers in flow field.

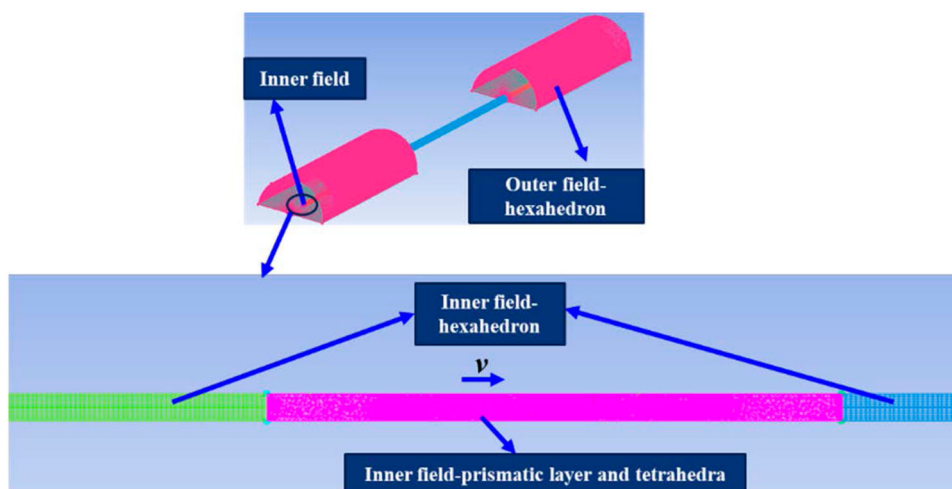|	Cd	Cs	Cl	Total cells
Fine mesh	0.0315	0.0013	0.0043	24 million
Medium mesh	0.0327	0.0015	0.0042	14 million
Coarse mesh	0.0336	0.0020	0.0049	10 million

Figure 4. Hybrid meshing for the flow field.

4. Results and discussion

The coupling effect between pantograph and tunnel was further analysed by comparison between the coupling of passing through a tunnel and the coupling of open air, and aerodynamics and multi-body dynamics passing through a tunnel were coupled or not, respectively.

A Chinese standard single-track tunnel was adopted. Its cross-sectional area is 70 m^2 and the 'unfavorable' tunnel length is 480 m. The speed is 360 km/h and the total distance is 800 m. Our primary research object is the pantograph, so the train was simplified in the flow field, on which some devices were ignored (air conditioners, bogies, shields). The flow field was divided into an inner field and outer field which is 3D, viscous, compressible, and unsteady turbulent. The hybrid meshing of this field is shown in Figure 4. The same grid was used for the inner field under different cases.

Aerodynamic simulations were conducted according to the real working conditions of the moving train and static ground. The displacement of the pantograph surface was taken from the multi-body dynamic calculation. The tunnel wall and ground were considered to be fixed walls. The boundaries of the calculation region were set as the pressure outlet and the outlet pressure was taken as standard atmospheric.

4.1. Coupling when passing through a tunnel versus coupling under open air

The proportions listed in this section are based on the calculation results of coupling under open air. The statistical results were recorded after removing the initial stage.

4.1.1. Time-domain characteristics

Figure 5 shows the comparison curves of time-domain characteristics between the coupling of passing through a tunnel and the coupling of open air, including the aerodynamic lift of the panhead, the contact force between the pantograph and catenary, the vertical displacement, and the vertical acceleration of the contact strip, respectively. Tables 3–5
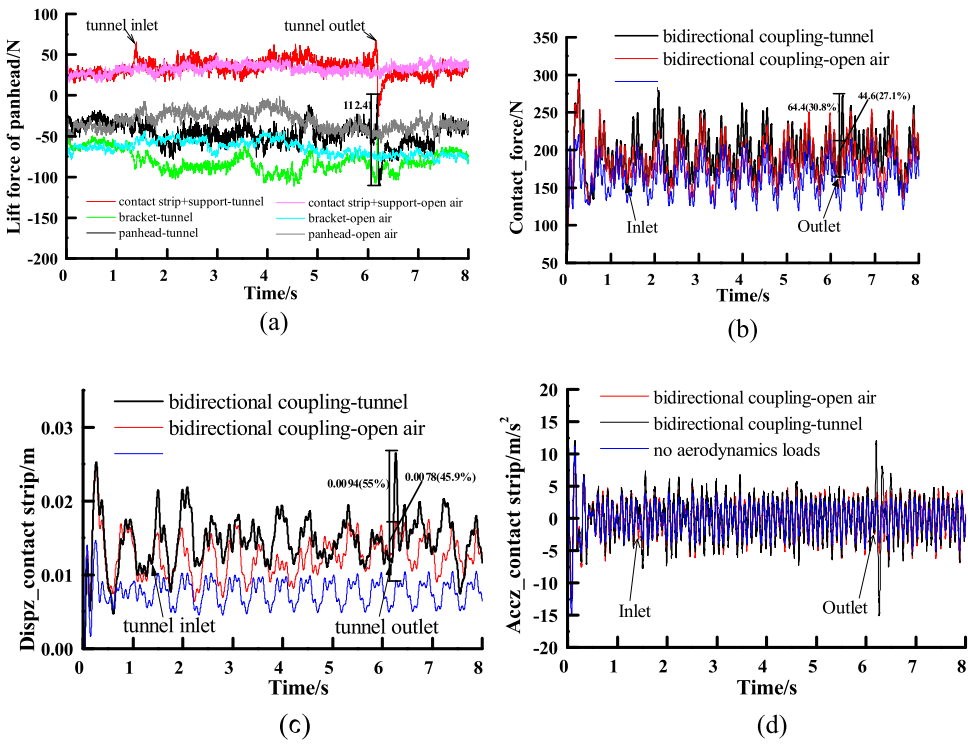
Figure 5. Comparison curves under the coupling of passing through a tunnel and the coupling of open air (a) the aerodynamic lift of the panhead; (b) the contact forces between pantograph and catenary; (c) the vertical displacement of the contact strip; (d) the vertical acceleration of the contact strip.

Table 3. Statistical results of the contact force between pantograph and catenary under the coupling of passing through a tunnel and the coupling of open air.

	Maximum (N)	Minimum (N)	Mean (N)	Standard deviation (N)	Standard deviation difference	Mean difference
Bidirectional coupling-tunnel	293.885	127.55	196.55243	28.08317	3.52%	6.49%
Bidirectional coupling-open air	289.73	126.475	184.56674	27.12849	–	–
No aerodynamics loads	221.09438	119.43517	162.95755	22.29535	−17.82%	−11.71%

provide statistical results for the contact force between the pantograph and catenary, the vertical displacement, and the vertical acceleration of the contact strip, respectively.

(1) Aerodynamic lift

The panhead of the pantograph is composed of a contact strip, support, and bracket. Aerodynamic lift is an important factor affecting the contact force between the pantograph and catenary. The curves in Figure 5(a) indicate that because of their geometric shapes, the directions of the aerodynamic lift of the contact strip-support are opposite to that of the bracket; the aerodynamic lift of the contact strip-support is smaller than that of the bracket.

Table 4. Statistical results of the vertical displacement of the contact strip under the coupling of passing through a tunnel and the coupling of open air.

	Maximum (m)	Minimum (m)	Mean (m)	Standard deviation (m)	Standard deviation difference	Mean difference
Bidirectional coupling-tunnel	0.0265	0.00469	0.01468	0.00331	18.21%	16.51%
Bidirectional coupling-open air	0.02501	0.00634	0.0126	0.0028	–	–
No aerodynamics loads	0.01468	0.00165	0.00764	0.00168	−40.00%	−39.37%

Table 5. Statistical results of the vertical acceleration of the contact strip under the coupling of passing through a tunnel and the coupling of open air.

	Maximum (m/s^2)	Minimum (m/s^2)	Mean (m/s^2)	Standard deviation (m/s^2)	Standard deviation difference	Minimum difference
Bidirectional coupling-tunnel	12.1125	−15.0945	0.0103	3.10342	17.63%	99.51%
Bidirectional coupling-open air	10.535	−7.56569	0.0115	2.63834	–	–
No aerodynamics loads	11.1128	−7.89158	0.01997	2.22724	−15.58%	4.31%

Compared with that under open air, when passing through a tunnel, the fluctuation amplitude of aerodynamic lift of the bracket is larger in the tunnel whereas the aerodynamic lift of contact strip-support is slightly different.

Further, compared with that under open air, when passing through a tunnel, the aerodynamic lift values do not significantly differ outside the tunnel at 0–1 s and 7.5–8 s. At this time, both are under open air; the calculation results are correct. The differences among aerodynamic lift values are larger compared to under open air at the entrance of the tunnel and largest at the exit. This can be attributed to a micro-pressure wave at the exit and significant differences between the interior and exterior of the tunnel. For example, at the exit, the aerodynamic lift of the panhead has a sudden change in amplitude of 112.41 N.

(2)   Contact force between pantograph and catenary

As shown in Figure 5(b) and Table 3, under the coupling of open air and the coupling of passing through a tunnel, the contact force between the pantograph and catenary is much smaller without than with aerodynamic loads. For example, the standard deviation and mean value are 17.82% and 11.71% smaller than that under the coupling of open air, respectively. Therefore, aerodynamic loads cannot be ignored. In the tunnel, the contact force between the pantograph and catenary under the coupling of passing through the tunnel is generally larger than that under open air, but it is opposite close to the tunnel exit. These phenomena are closely related to the change laws of aerodynamic lift of the panhead under the two cases.

Compared with that under the coupling of open air, under the coupling of passing through a tunnel, the standard deviation and the mean of the contact force are 3.52% and 6.49% larger, respectively. However, the contact force at the exit and some positions in the tunnel is much larger; at 6.27 s, for example, the value is 64.4 N larger and the

corresponding proportion is 30.8%. At this time, the impact between the pantograph and catenary at these positions is also much larger and the current collection quality degrades significantly. These points should be prioritised in the pantograph design.

(3)   Vertical displacement of contact strip

As shown in Figure 5(c) and Table 4, under the coupling of passing through a tunnel and that of open air,the vertical displacement of the contact strip is much smaller and steadier without considering aerodynamics loads than with this consideration. For example, the standard deviation and the mean value are 40.00% and 39.37% smaller than that of the coupling of open air, respectively. Therefore, the aerodynamic loads cannot be ignored.

In the tunnel, the vertical displacement of the contact strip under the coupling of passing through a tunnel is basically larger than that under the coupling of open air, but it is opposite close to the tunnel exit. These are closely related to the change laws of aerodynamic lift of the panhead under the two cases. Compared with that under the coupling of open air, under the coupling of passing through a tunnel, the standard deviation and the mean of the vertical displacement of the contact strip are 18.21% and 16.51% larger, respectively. However, the vertical displacement of the contact strip at the exit and some positions in the tunnel is much larger. At 6.27 s, for example, the value is 0.0094 m larger and the corresponding proportion is 55%. These phenomena are closely associated with the aerodynamic lift.

(4)   Vertical acceleration of contact strip

As shown in Figure 5(d) and Table 5, under the coupling of open air and the coupling of passing through a tunnel, without aerodynamics loads, the vertical acceleration of the contact strip is much smaller than with aerodynamics loads. For example, the standard deviation and the mean value are 15.58% and 4.31% smaller than that under the coupling of open air, respectively. The influence of aerodynamic lift on the vertical acceleration of the contact strip is less intense than that on the vertical displacement or contact force.

In the tunnel, the vertical acceleration of the contact strip under the coupling of passing through the tunnel is larger than that under the coupling of open air, but it is opposite close to the tunnel exit. These phenomena are closely related to the change laws of aerodynamic lift of the panhead under the two cases. Compared with that under the coupling of open air, under the coupling of passing through a tunnel, the standard deviation and minimum of the contact strip vertical acceleration are 17.63% and 99.51% larger, respectively. The tunnel effect is significant.

4.1.2. Frequency-domain characteristics

Under the coupling of passing through a tunnel and the coupling of open air, the power spectral density curves of the contact force between the pantograph and catenary, as well as the vertical displacement and acceleration of the contact strip are shown in Figure 6. The basic frequencies of the three characteristics are all 2.11 Hz and there are multiple frequencies. Under three cases, the change laws of the frequency-spectrum of three characteristics are basically consistent. It indicates the aerodynamic loads do not change the main frequencies of the pantograph structure.
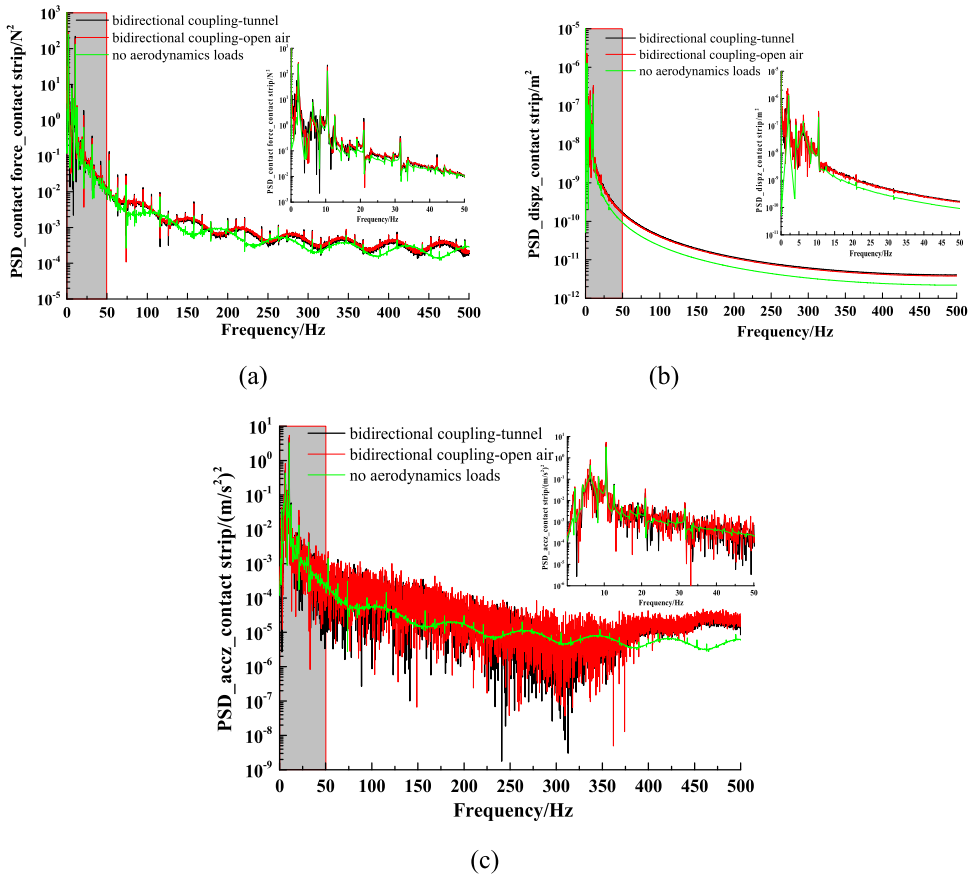
(a)   (b)

(c)

Figure 6. Power spectral density curves under the coupling of passing through a tunnel and the coupling of open air (a) the contact force between pantograph and catenary; (b) the vertical displacement of the contact strip; (c) the vertical acceleration of the contact strip.

At the basic frequency, the 5× frequency, 10× frequency, 15× frequency … , the amplitudes are larger for the contact force between the pantograph and catenary. The line test data after 20 Hz filtering is insufficient for the high-speed pantograph. The change trends of the contact force between pantograph and catenary under three cases are not completely consistent when the frequency exceeds 50 Hz. The amplitude of the vertical displacement of the contact strip also are larger at the basic frequency, the 5× frequency, 10× frequency, and 15× frequency. Its main frequencies are mainly concentrated in the low frequency range (below 25 Hz). Over 50 Hz, the main frequencies of the vertical acceleration of the contact strip are not obvious, but are larger when the aerodynamics loads are considered.

4.2. Coupled versus un-coupled aerodynamics and multi-body dynamics passing through a tunnel

4.2.1. Time-domain characteristics
Figure 7 shows comparison curves of the aerodynamic lift of the panhead, the contact force between the pantograph and catenary, and the vertical displacement and acceleration of
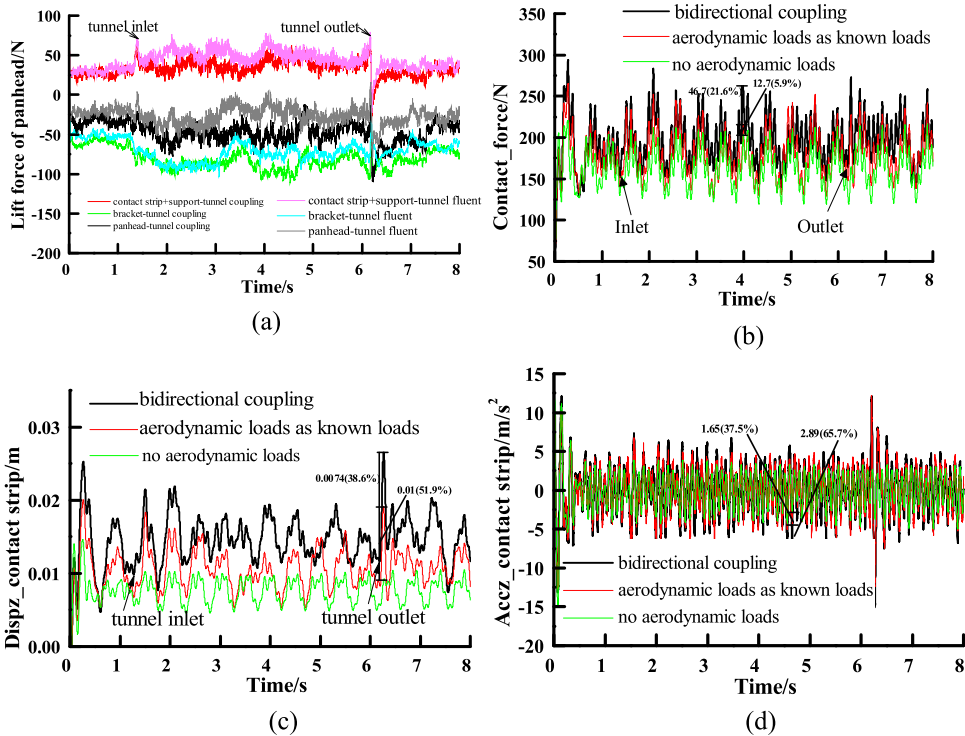
Figure 7. Comparison curves with and without coupling of aerodynamics and multi-body dynamics passing through a tunnel (a) the aerodynamic lift of the panhead; (b) the contact force between pantograph and catenary; (c) the vertical displacement of the contact strip; (d) the vertical acceleration of the contact strip.

the contact strip with versus without coupling of aerodynamics and multi-body dynamics passing through a tunnel. Tables 6–8 show the statistical results of the contact force between the pantograph and catenary as well as the vertical displacement and acceleration of the contact strip.

(1)   Aerodynamic lift

The 'single aerodynamic calculation case' denotes a lack of coupling between aerodynamics and multi-body dynamics. As shown in Figure 7(a), due to their geometric shapes, the directions of the aerodynamic lift of the contact strip-support are opposite to that of the bracket, and the aerodynamic lift of the contact strip-support is smaller than that of the bracket (except at the exit of the tunnel). At a certain distance from the entrance and the exit to the tunnel (i.e. 0–1 s and 7.5–8 s), all the aerodynamic lifts are similar. Both are under open air at these time points, which indicates that the calculation results are correct.

In the middle and rear of the tunnel, the aerodynamic lift values of the bracket and the panhead differ to greater extent. The differences of the contact strip-support are opposite. In both cases, the differences of all aerodynamic lift values are larger at the entrance of the tunnel and the largest at the exit. This can be attributed to the micro-pressure wave at the exit and the significant differences between the exterior and interior of the tunnel.

Table 6. Statistical results of the contact force between pantograph and catenary with and without coupling of aerodynamics and multi-body dynamics passing through the tunnel.

	Maximum (N)	Minimum (N)	Mean (N)	Standard deviation (N)	Standard deviation difference	Mean difference
Bidirectional coupling-tunnel coupling	293.885	127.55	196.55243	28.08317	6.69%	8.30%
Aerodynamics loads as known loads	265.72046	127.28857	180.24632	26.3219	–	–
No aerodynamics loads	221.09438	119.43517	162.95755	22.29535	−15.30%	−9.59%

(2) Contact force between pantograph and catenary

When aerodynamics and multi-body dynamics passing through a tunnel are not coupled, aerodynamics loads are considered as known loads. As shown in Figure 7(b) and Table 6, the contact force between the pantograph and catenary is much smaller without the aerodynamics loads than when aerodynamics loads are 'known' and the aerodynamics and multi-body dynamics are coupled. For example, the standard deviation and mean are 15.30% and 9.59% smaller without the aerodynamics loads than under the case of known aerodynamics loads. Therefore, the aerodynamic loads cannot be ignored.

In the tunnel, the contact force between the pantograph and catenary under the coupling of passing through a tunnel is generally larger than that under the case of aerodynamics loads as known loads, but the opposite is true close to the tunnel exit. These phenomena are closely related to the change laws of aerodynamic lift of the panhead under the two cases. Compared with that under the case of aerodynamics loads as known loads, under the coupling of passing through the tunnel, the standard deviation and mean of contact force are 6.69% and 8.30% larger, respectively. At the exit and some other positions in the tunnel, the contact force is much larger; for example, at 4.0 s, the value is 46.7 N larger and the corresponding proportion is 21.6%. At this point, the impact between the pantograph and catenary at these positions is also much larger and the current collection quality degrades. These points should be prioritised in the pantograph design.

(3) Vertical displacement of contact strip

As shown in Figure 7(c) and Table 7, the vertical displacement of the contact strip is much smaller and steadier when aerodynamics loads are not considered rather than aerodynamics and multi-body dynamics are coupled and considering aerodynamics loads to be known. For example, the standard deviation and mean are 37.08% and 28.60% smaller than that under the case of aerodynamics loads as known loads, respectively. Therefore, the aerodynamic loads cannot be ignored.

In the tunnel, the vertical displacement of the contact strip under the coupling of passing through a tunnel is larger than that under the case of aerodynamics loads as known loads. Compared with that under the case of aerodynamics loads as known loads, under the coupling of passing through a tunnel, the standard deviation and mean of the vertical displacement of the contact strip are 23.97% and 37.20% larger, respectively. The coupling effect between aerodynamics and multi-body dynamics is significant. The vertical displacement of the contact strip at the exit and some positions in the tunnel is much larger, e.g.

Table 7. Statistical results of the vertical displacement of the contact strip with and without coupling of aerodynamics and multi-body dynamics passing through the tunnel.

	Maximum (m)	Minimum (m)	Mean (m)	Standard deviation (m)	Standard deviation difference	Mean difference
Bidirectional coupling-tunnel coupling	0.0265	0.00469	0.01468	0.00331	23.97%	37.20%
Aerodynamics loads as known loads-tunnel	0.02003	0.00353	0.0107	0.00267	–	–
No aerodynamics loads	0.01468	0.00165	0.00764	0.00168	−37.08%	−28.60%

Table 8. Statistical results of the vertical acceleration of the contact strip with and without coupling of aerodynamics and multi-body dynamics passing through the tunnel.

	Maximum (m/s^2)	Minimum (m/s^2)	Mean (m/s^2)	Standard deviation (m/s^2)	Standard deviation difference	Minimum difference
Bidirectional coupling-tunnel	12.1125	−15.0945	0.0103	3.10342	12.42%	21.65%
Aerodynamics loads as known loads-tunnel	12.21301	−12.40814	0.00425	2.7605	–	–
No aerodynamics loads	11.1128	−8.52439	0.01885	2.22931	−19.24%	−31.30%

0.0074 m larger at 6.27s where the corresponding proportion is 38.6%. These phenomena are closely associated with aerodynamic lift.

(4)   Vertical acceleration of contact strip

As shown in Figure 7(d) and Table 8, the vertical acceleration of the contact strip is much smaller without considering aerodynamics loads compared with that under the case of aerodynamics loads as known loads and the coupling case of aerodynamics and multi-body dynamics. For example, the standard deviation and minimum are 19.24% and 31.30% smaller than that under the case of aerodynamics loads as known loads, respectively. Thus, aerodynamic loads cannot be ignored.

In the tunnel, the vertical acceleration of the contact strip under the coupling of passing through a tunnel is basically larger than that under the case of known aerodynamics loads. Compared with that under the case of aerodynamics loads as known loads, under the coupling of passing through a tunnel, the standard deviation and minimum of vertical acceleration of the contact strip are 12.42% and 21.65% larger, respectively. The vertical acceleration of the contact strip is much larger at the exit and at certain positions in the tunnel. For example, at 4.65 s, the value is 2.89 m/s^2 larger and the corresponding proportion is 65.70%. These phenomena are closely related to the change laws of aerodynamic lift of the panhead under the two cases. Thus, the coupling effects between aerodynamics and multi-body dynamics and between the pantograph and tunnel are significant.

4.2.2. Frequency-domain characteristics

Under the coupling of passing through a tunnel, the case of aerodynamic loads as known loads, and the case without aerodynamics loads, the power spectral density curves of the
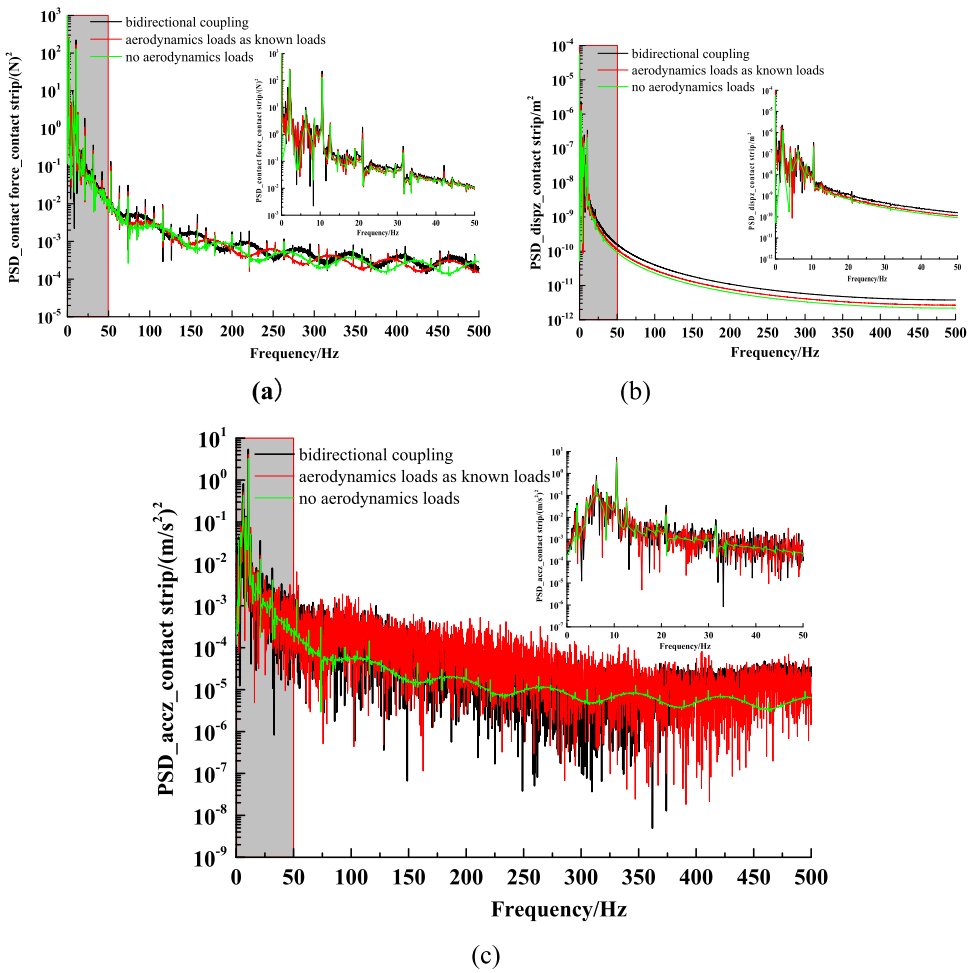
Figure 8. Power spectral density curves under different cases of passing through a tunnel (a) the contact force between pantograph and catenary; (b) the vertical displacement of the contact strip; (c) the vertical acceleration of the contact strip.

contact force between pantograph and catenary, the vertical displacement and acceleration of the contact strip are shown in Figure 8, respectively. It can be seen as follows from the curves.

The basic frequencies of the three characteristics are 2.11 Hz and there are multiple frequencies. The change laws of the frequency-spectrum of the three characteristics are basically consistent across all cases, which indicates that aerodynamic loads do not change the main frequencies of the pantograph structure. There are relatively high frequencies for the contact force between the pantograph and catenary. The line test data after 20 Hz filtering is insufficient for high-speed pantographs. The change trends of the three cases are not completely consistent when the frequency exceeds 50 Hz.

The vertical displacement amplitude of the contact strip is larger at the basic frequency, 5× frequency, 10× frequency, and 15× frequency. Its main frequencies are mainly concentrated in the low frequency range (below 25 Hz). The vertical acceleration amplitude

of contact strip is larger significantly at $3\times$ frequency. Over 50 Hz, its main frequencies are not obvious; however, its amplitudes are larger, when the aerodynamics loads are considered.

5. Conclusions

A precise and efficient coupling method between aerodynamics and multi-body dynamics was developed to study current collection quality for trains passing through tunnels at high speed. The coupling effect between the pantograph and tunnel was analysed accordingly. Our main conclusions can be summarised as follows.

(1) Aerodynamic lift significantly influences the amplitudes of many pantograph characteristics. It is an important factor affecting the contact state between the pantograph and catenary and cannot be reasonably neglected. However, it does not affect the main frequencies of the pantograph structure. The coupling effect between the pantograph and tunnel is significant.
(2) Compared with that under the coupling case of open air, under the coupling case of passing through a tunnel, the standard deviation and mean of the contact force are 3.52% and 6.49% larger, respectively. The standard deviation and mean of the vertical displacement of the contact strip are 18.21% and 16.51% larger, respectively. The standard deviation and minimum of the vertical acceleration of the contact strip are 17.63% and 99.51% larger, respectively.
(3) Compared with that under the case of known aerodynamic loads, under the coupling of passing through the tunnel, the standard deviation and mean of the contact force are 6.69% and 8.30% larger, respectively. The standard deviation and mean of the vertical displacement of the contact strip are 23.97% and 37.20% larger, respectively. The standard deviation and minimum of the vertical acceleration of the contact strip are 12.42% and 21.65% larger, respectively.
(4) All basic frequencies of these characteristics are 2.11 Hz. There are multiple frequencies. Higher frequencies occur in high-speed pantographs for the contact force between the pantograph and catenary.

Disclosure statement

Funding

References

[1] Dai ZY, Li T, Deng J, et al. Effect of the strip spacing on the aerodynamic performance of a high-speed double-strip pantograph. Veh Syst Dyn. 2021. doi:10.1080/00423114.2021.1945117.
[2] Li T, Qin D, Zhang WH, et al. Study on the aerodynamic noise characteristics of high-speed pantographs with different strip spacings. J Wind Eng Ind Aerodyn. 2020;202:10419.

[3] Dai ZY, Li T, Zhang WH, et al. Numerical study on aerodynamic performance of high-speed pantograph with double strips. Fluid Dyn Mater Process. 2020;16(1):31–40.

[4] He DD, Gao Q, Zhong WX. A numerical method based on the parametric variational principle for simulating the dynamic behavior of the pantograph-catenary system. Shock Vib. 2018. doi:10.1155/2018/7208045.

[5] Song DL, Jiang YN, Zhang WH. Dynamic performance of a pantograph–catenary system with consideration of the contact surface. Proc Inst Mech Eng F J Rail Rapid Transit. 2018;232(1):262–274.

[6] Van OV, Massat JP, Balmes E. Waves, modes and properties with a major impact on dynamic pantograph-catenary interaction. J Sound Vib. 2017;402:51–69.

[7] Gregori S, Tur M, Nadal E, et al. Fast simulation of the pantograph–catenary dynamic interaction. Finite Elem Anal Des. 2017;129:1–13.

[8] Lee JH, Park TW, Oh HK, et al. Analysis of dynamic interaction between catenary and pantograph with experimental verification and performance evaluation in new high-speed line. Veh Syst Dyn. 2015;53(8):1117–1134.

[9] Nåvik P, Rønnquist A, Stichel S. Variation in predicting pantograph–catenary interaction contact forces, numerical simulations and field measurements. Veh Syst Dyn. 2017;55(9):1265–1282.

[10] Wang H, Núñez A, Liu Z, et al. Analysis of the evolvement of contact wire wear irregularity in railway catenary based on historical data. Veh Syst Dyn. 2018;56(8):1207–1232.

[11] Carnevale M, Facchinetti A, Maggiori L, et al. Computational fluid dynamics as a means of assessing the influence of aerodynamic forces on the mean contact force acting on a pantograph. Proc Inst Mech Eng F J Rail Rapid Transit. 2016;230(7):1698–1713.

[12] Pombo J, Ambrósio J. Environmental and track perturbations on multiple pantograph interaction with catenaries in high-speed trains. Comput Struct. 2013;124:88–101.

[13] Kulkarni S, Pappalardo CM, Shabana AA. Pantograph/catenary contact formulations. J Vib Acoust. 2017;139(1):1–12.

[14] Song Y, Liu ZG, Wang HR, et al. Nonlinear analysis of wind-induced vibration of high-speed railway catenary and its influence on pantograph–catenary interaction. Veh Syst Dyn. 2016;54(6):723–747.

[15] Li RP, Zhang WH, Ning Z, et al. Influence of a high-speed train passing through a tunnel on pantograph aerodynamics and pantograph–catenary interaction. Proc Inst Mech Eng F J Rail Rapid Transit. 2017;231(2):198–210.

[16] Shi HJ, Chen G, Yang YR. A comparative study on pantograph-catenary models and effect of parameters on pantograph-catenary dynamics under crosswind. J Wind Eng Ind Aerodyn. 2021;211:1–18.

[17] Nakade K, Masahiro S, Hiroshi F. Interaction between vehicle vibration and aerodynamic force on high-speed train running in tunnel. Veh Syst Dyn. 2004;41:717–723.

[18] Li T, Zhang JY, Zhang WH. An improved algorithm for fluid-structure interaction of high-speed trains under crosswind. J Mod Transp. 2011;19(2):75–81.

[19] Mandal A, Maity D. Seismic analysis of dam-foundation-reservoir coupled system using direct coupling method. Coupled Syst Mech. 2019;8(5):393–414.

[20] Zheng HX, Wang JS. A numerical study on the flow-induced vibrations of flexible cylinders attached with fixed short fairings. Ocean Eng. 2021;229:1–20.

[21] Huang CD. Aaeroelasticity research based on CFD/CSD coupling considering structural nonlinearity [dissertation]. Beijing: Institute of Mechanics, Chinese Academy of Sciences; 2017.

[22] Mittal K, Dutta S, Fischer P. Multirate timestepping for the incompressible Navier-Stokes equations in overlapping grids. J Comput Phys. 2021;437:1–21.

[23] Hu ZY, Xu GH, Shi YJ. A robust overset assembly method for multiple overlapping bodies. Int J Numer Methods Fluids. 2021;3(93):653–682.

[24] Sharma A, Ananthan S, Sitaraman J, et al. Overset meshes for incompressible flows: on preserving accuracy of underlying discretizations. J Comput Phys. 2021;428:1–29.